Journal of Alloys and Compounds 623 (2015) 96–103

Contents lists available at ScienceDirect

Journal of Alloys and Compounds

journal homepage: www.elsevier.com/locate/jalcom

Solute redistribution during annealing of a cold rolled Cu–Ag alloy

J. Gubicza [a,*], Z. Hegedűs [a,b], J.L. Lábár [a,c], A. Kauffmann [d,e], J. Freudenberger [d,f], V. Subramanya Sarma [g]

[a] Department of Materials Physics, Eötvös Loránd University, Budapest, P.O.B. 32, H-1518, Hungary
[b] Max Planck Institute for Intelligent Systems, Heisenbergstrasse 3, D-70569 Stuttgart, Germany
[c] Research Institute for Technical Physics and Materials Science, Research Centre for Natural Sciences, Hungarian Academy of Sciences, P.O. Box 49, H-1525 Budapest, Hungary
[d] IFW Dresden, P.O. Box 270116, 01171 Dresden, Germany
[e] TU Dresden, Institute of Materials Science, 01062 Dresden, Germany
[f] TU Bergakademie Freiberg, Institute of Materials Science, Gustav-Zeuner-Str. 5, 09599 Freiberg, Germany
[g] Department of Metallurgical and Materials Engineering, Indian Institute of Technology Madras, Chennai 600036, India

ARTICLE INFO

Article history:
Received 6 July 2014
Received in revised form 17 August 2014
Accepted 21 October 2014
Available online 27 October 2014

Keywords:
Nanostructured materials
Dislocations and disclinations
Microstructure
Transmission electron microscopy
TEM
X-ray diffraction

ABSTRACT

Supersaturated Cu–3 at.% Ag alloy was rolled at liquid nitrogen temperature and then annealed at 623 K up to 120 min. The evolution of the microstructure as a function of annealing time was studied. In the initial stage of the heat-treatment a heterogeneous microstructure was developed where both the dislocation density and the solute Ag concentration in the Cu matrix varied considerably. In the regions where the initial Ag particles have a very small size and/or large Cu/Ag interface energy, dissolution occurred due to the Gibbs–Thomson effect while in other volumes the solute Ag concentration decreased to the equilibrium level. In the regions where the solute Ag concentration increased due to dissolution, a considerable fraction of dislocations formed during rolling was retained in the Cu matrix after annealing. In the volumes where the solute Ag content decreased due to precipitation, significant reduction in the dislocation density was observed. The evolution and the stability of this heterogeneous microstructure were investigated experimentally and discussed using model calculations.

1. Introduction

The mechanical properties of metallic materials can be improved by severe plastic deformation (SPD) techniques [1,2]. The increase in the lattice defect densities (such as dislocations) and the grain refinement during SPD result in enhancement of strength. The SPD-induced strength can be further improved by alloying as the additive elements have a pinning effect on dislocations and grain boundaries [3–5]. Solute atoms increase the critical resolved shear stress needed for dislocation glide which can be expressed as $\Delta\tau = 0.0014G\delta^{3/2}c^n$, where G is the matrix shear modulus, δ is the relative change of lattice constant of the matrix per unit solute atom concentration and the exponent n equals 1/2 and 2/3 for dilute and more concentrated solid solutions, respectively [6]. The strengthening effect of solute atoms increases with increasing the difference between the atomic radii of solute and solvent atoms. However, for dilute alloys the shear strength increment usually remains under 10 MPa, even if the atomic radius difference reaches 15–20%, as for instance in the cases of Al–Mg or Cu–Ag binary systems [7]. At the same time, the solute atoms have an indirect hardening effect by increasing the density of dislocations due to hindering their annihilation. It has been shown [8] that 1 and 3 at.% Mg in severely deformed Al yielded a two and twelve fold rise in dislocation density, respectively. In the latter case, the shear stress increment due to the rise of the dislocation density was one order of magnitude larger than the direct hardening effect of Mg solute atoms. When the alloying elements form precipitates, the annihilation of dislocations is also hindered, but this effect strongly depends on the size and the distribution of precipitates in the matrix, as well as on the nature of interface between the matrix and the secondary particles. If the spacing between the precipitates is larger than the distance between dislocations with opposite signs and/or the interfaces are coherent or semicoherent (i.e. the precipitates are shearable), the secondary particles only weakly hinder the dislocation annihilation.

The concentration of the alloying element before SPD can be raised even to the supersaturated level via a solution heat-treatment and subsequent quenching which further increases the mechanical strength [9]. However, it was also revealed that the increase of the strength in SPD-processed ultrafine-grained (UFG) materials is accompanied by a reduction of the tensile ductility due to the loss of strain hardening capacity of the samples [10]. Short-time heat-treatments after SPD were successfully applied

* Corresponding author. Tel.: +36 1 372 2876; fax: +36 1 372 2811.
E-mail address: jeno.gubicza@ttk.elte.hu (J. Gubicza).

http://dx.doi.org/10.1016/j.jallcom.2014.10.093
0925-8388/

in order to increase the ductility considerably while retaining the high strength [11,12]. During annealing following SPD-processing usually a heterogeneous structural relaxation (i.e. recovery and recrystallization) occurs. Therefore, during a subsequent tensile test the dislocation density can increase in the relaxed volumes, leading to a considerable strain hardening which results in an improved ductility of the material.

Cu–Ag alloys have important practical applications such as conductor materials in high-field magnets [13,14]. The requirements for conductor materials in pulsed high field magnets are the followings: high mechanical strength in order to resist Lorentz force, high electrical conductivity to prevent Joule's heating and reasonable ductility in order to allow coil winding [15]. SPD-processing of Cu–Ag alloys can improve their strength [16–18], however the ductility is usually reduced concomitantly [17,19]. A recent report [17] has shown that a combination of high strength and good ductility can be achieved in supersaturated Cu–3 at.% Ag alloy by annealing after rolling at liquid nitrogen temperature (LNT). This cryo-rolled sample exhibited high ultimate tensile strength (UTS) with the value of ~710 MPa and negligible uniform elongation (~1%). After annealing for 5 min at 648 K, the UTS decreased only by ~60 MPa while the uniform elongation was significantly improved from 1% to 8%. These changes in the mechanical properties were attributed to the partial recovery and/or recrystallization of the UFG microstructure. However, a systematic study of the evolution of the phase composition and the defect structure during annealing of SPD-processed supersaturated Cu–Ag alloys is missing from the literature.

In this paper, the evolution of the microstructure in cryo-rolled Cu–3 at.% Ag alloy during isothermal annealing at 623 K up to 120 min is studied in detail. The processes leading to the formation of an inhomogeneous microstructure are described experimentally and discussed theoretically. It will be shown that the heterogeneity of the dislocation structure is mainly caused by the development of an inhomogeneous solute Ag concentration in the initial stages of annealing. This investigation also reveals the thermal stability of the cryo-rolled microstructure in supersaturated Cu–3 at.% Ag alloy which is an important issue from the point of view of practical applications of this SPD-processed material.

2. Material and methods

Cu–3 at.% Ag alloy was prepared by induction melting in Ar atmosphere from high purity (99.9%) elements and casting them into $15 \times 15 \times 150$ mm^3 graphite moulds. The alloy was homogenized at 750 °C (1023 K) for 5 h and subsequently water quenched. The homogenized plate was subjected to cryo-rolling at LNT (~77 K). The starting and the final thicknesses were 15 and 2 mm, respectively. The thickness reduction was achieved in multiple passes with about 10% reduction per pass. After each pass, the plate was immersed in liquid nitrogen for 2 min before further reduction. The rolls were not cooled. The total thickness reduction was 85% which corresponds to a logarithmic strain of ~2. Liquid nitrogen cooling ensures that the heating of the sample during cold work does not yield a temperature rise that might cause recovery or recrystallization.

Analysis of differential scanning calorimetry measurements at a heating rate of 10 K/min showed that recovery and recrystallization in the cryo-rolled sample start in the region of ~623–648 K [17]. In order to investigate the evolution of the microstructure during annealing, cryo-rolled samples were heat-treated isothermally at 623 K for 5, 10, 15, 20, 30, 45, 60, 75, 90 and 120 min. The effect of this annealing on the microstructure was investigated by X-ray diffraction (XRD). The variation of the solute Ag concentration in the Cu matrix due to annealing was determined from the change of the lattice parameter as obtained by XRD using a Philips Xpert Θ–2Θ powder diffractometer with Cu Kα radiation (wavelength: $\lambda = 0.15418$ nm). The lattice constant was calculated by the Nelson–Riley extrapolation method [20].

The microstructure in the Cu matrix was characterized by X-ray line profile analysis (XLPA). For this investigation the X-ray diffraction patterns were measured by a high-resolution rotating anode diffractometer (type: RA-MultiMax9, manufacturer: Rigaku) using Cu $K\alpha_1$ ($\lambda = 0.15406$ nm) radiation. The surface area of the samples irradiated by X-rays was 4×10^{-5} m^2 which is about nine orders of magnitude larger than the characteristic structural element areas (e.g. the square of the crystallite size or the square of the average dislocation distance). Therefore, the XLPA measurements have very good statistics. For each sample only one measurement was performed, as our former experiments have revealed that the repeated measurements yielded smaller deviations in the results than the uncertainties in the evaluation of a single X-ray diffraction pattern. Two-dimensional imaging plates were used to detect the Debye–Scherrer diffraction rings. The line profiles (perpendicular to the rings) were obtained by integrating the two dimensional intensity distribution along the rings. The X-ray diffraction line profiles were evaluated for the microstructure by the extended Convolutional Multiple Whole Profile (eCMWP) fitting method [21]. In this procedure, the diffraction pattern is fitted by the sum of a background spline and the convolution of the instrumental pattern and the theoretical line profiles related to the crystallite size, dislocations and twin faults. In the calculation of the theoretical profile functions it is assumed that the crystallites have spherical shape with log-normal size distribution and the strain is caused by dislocations. Strain anisotropy is taken into account by the dislocation contrast factors. In order to increase the speed of the eCMWP procedure, instead of the convolution of the different profile components caused by the microstructure, each theoretical peak profile is calculated as the inverse Fourier transformation of the product of the theoretical size, dislocation and twin faulting Fourier transforms. In the cases of size and dislocation broadening, the Fourier transforms of the profiles can be expressed in analytical forms, as shown in Refs. [22,23], respectively. The Fourier transform of each reflection caused by twin faults can be calculated as the sum of the Fourier transforms of the different subreflections [24]. More details about the eCMWP procedure can be found in Refs. [21,22]. As an example, the fitting for the cryo-rolled specimen is shown in Fig. 1. The following characteristic quantities of the microstructure were obtained from the eCMWP fitting procedure: the median and the log-normal variance of the crystallite size distribution, the dislocation density and the twin boundary probability. The area-weighted mean crystallite size ($\langle x \rangle_{area}$) was calculated from the median (m) and the log-normal variance (σ^2) of the assumed log-normal crystallite size distribution as: $\langle x \rangle_{area} = m \cdot \exp(2.5\sigma^2)$. The twin boundary probability is defined as the fraction of twin faults among the {1 1 1} lattice planes.

Complementary transmission electron microscopy (TEM) investigations were carried out on the cryo-rolled specimen and the samples annealed at 623 K for short (10 and 20 min) and long (120 min) times. TEM lamellae were prepared with special care to avoid additional unwanted annealing of the samples. Low temperature glue (GATAN G1) was used at 60 °C to fix the sample in the 3 mm diameter Ti disk. Ion milling was carried out at 7 keV with continuous cooling of the sample by liquid nitrogen. TEM examinations were performed in a JEOL 3010 operated at 300 keV. Images and diffraction patterns were recorded with a GATAN Orius camera. The diffraction patterns were indexed with the help of the ProcessDiffraction program [25]. Distances in the Moiré pattern were measured with the commercial Digital Micrograph program.

3. Results

The Ag solute content in the Cu matrix was determined from the lattice parameter measured by XRD. The relative experimental error of the lattice parameter for the alloy was only about 3×10^{-4}. However, the deviation of the alloy lattice constant from the value characteristic for pure Cu was about three orders of magnitude smaller than the lattice parameter itself. Therefore, the relative error of the solute Ag content was as large as 10–30%. According to Ref. [26], the lattice constant dependence on Ag concentration in Cu can be described by a second-order polynomial. However, for dilute alloys (at least up to 10% Ag concentration) this

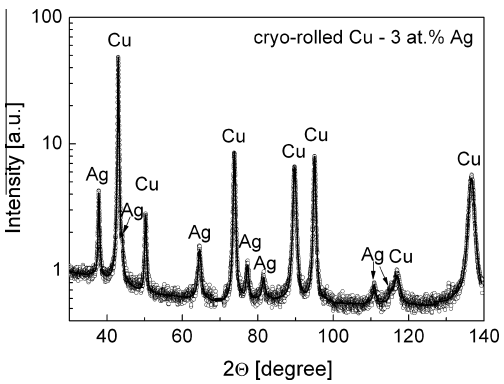

Fig. 1. The fitting of the X-ray diffraction pattern for the cryo-rolled Cu–3 at.% Ag by the eCMWP method. The open circles and the solid line represent the measured data and the fitted curves, respectively. The intensity is in logarithmic scale.

relationship can be well approximated by a linear function in which 1 at.% Ag in solution yields an increment of ~0.0007 nm in the lattice parameter of Cu (the lattice parameter of pure Cu is 0.3615 nm). Based on this, the Ag concentration in the Cu matrix of the cryo-rolled sample was determined to be 1.0 ± 0.1 at.%. As the total concentration of Ag in the base alloy is 3 at.%, about 2 at.% Ag is expected to be present as secondary Ag-rich phase. Indeed, Ag peaks were observed in the XRD pattern of the cryo-rolled sample (see Fig. 1). According to the equilibrium phase diagram of the Cu–Ag system, the solubility limit of Ag in Cu is 4 at.% at 750 °C, therefore during the homogenization heat-treatment all Ag atoms were dissolved in the Cu matrix. The Ag precipitates observed in the as-rolled samples most probably developed during cryo-rolling, as SPD-processing could promote precipitation [27]. The SPD-induced precipitates are favorably formed at lattice defects (e.g. at dislocations), therefore their chemical composition and interface structure may differ from those observed in an undistorted lattice. Nevertheless, the Cu matrix with ~1 at.% solute Ag concentration after rolling is in supersaturated state since the equilibrium solubility limit of Ag in Cu is below 0.1 at.% at RT.

The microstructural parameters of the Cu matrix in the cryo-rolled sample were obtained by XLPA. The crystallite size in the as-rolled condition (~30 nm) is much smaller and the dislocation density is significantly higher (~48×10^{14} m^{-2}) than the values reported in pure Cu processed by different SPD methods [28–30]. This observation can be explained by the pinning effect of Ag on dislocations and grain boundaries formed during SPD and the low temperature of deformation (LNT). The twin boundary probability was 0.5 ± 0.1%. The UFG microstructure in the rolled material is illustrated in the TEM image of Fig. 2a taken in the RD-TD plane (RD: rolling direction, TD: transverse direction). It should be noted that the grain size is much larger than the crystallite size obtained by XLPA which is in accordance with earlier studies and can be explained by the fact that the crystallite size usually corresponds to the subgrain size in severely deformed microstructures [31]. The dark-field TEM image in Fig. 2b was obtained for the cryo-rolled sample using an Ag reflection. In this area the Ag precipitates are equiaxed with the size of a few nanometers.

After annealing the cryo-rolled sample, each diffraction peak of the Cu matrix splits into two components. As an example, Fig. 3 shows reflection (220) for the sample annealed for 20 min. For comparison, the same reflection for the cryo-rolled specimen is also presented. The splitting of the peaks is probably caused by the development of an inhomogeneous solute atom distribution in the Cu matrix during annealing, resulting in a variation of the lattice parameter of the Cu matrix. Each line profile was evaluated by fitting it with the sum of two profile components having different Bragg-angles which correspond to two distinct regions of the matrix having different average lattice parameters. It should be noted that most probably the description of the distribution of the solute concentration by only two distinct solute contents is a simplification. Nevertheless, this procedure characterizes the inhomogeneity of the chemical composition of the matrix. The Ag solute concentrations in the two regions of the matrix have been determined from the lattice parameters of the two Cu phases obtained from the sub-profile positions and shown as a function of annealing time in Fig. 4a. It is noted that the solid curves in Fig. 4 serve only as guide to eyes. The volumes with low and high Ag contents are referred to as Regions 1 and 2, respectively. The peaks of Regions 1 and 2 are at higher and lower diffraction angles, respectively. In Region 2, the solute Ag content increased from ~1 at.% to 2.6 ± 0.3 at.% within 5 min annealing and it decreased slightly to 1.9 ± 0.3 at.% with increasing annealing time up to 75 min. For longer durations of heat-treatment the solute Ag concentration in Region 2 was not determined due to the low volume fraction of this region (see below). In Region 1, the solute Ag concentration

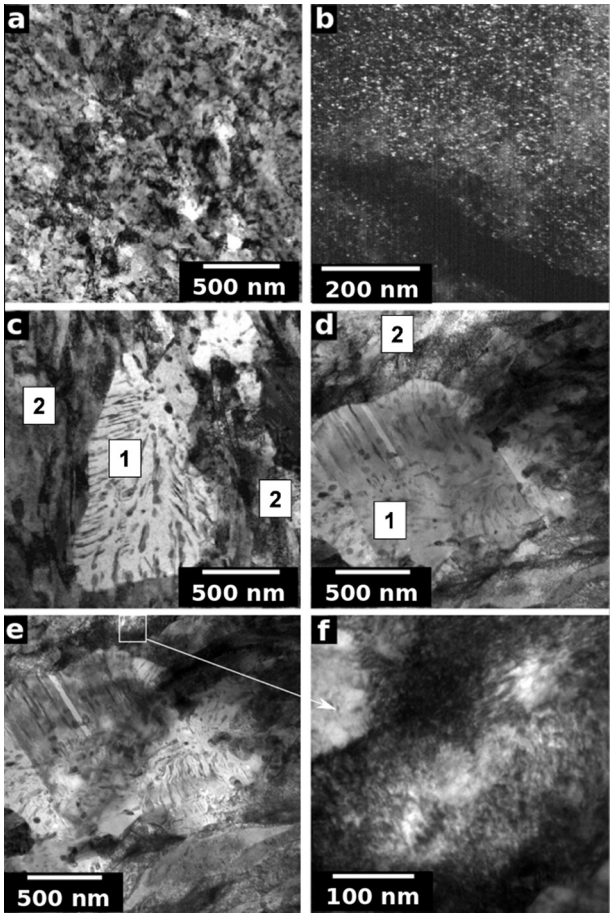

Fig. 2. TEM bright-field images of the microstructure in the cryo-rolled state (a), and after annealing for short times of 10 min (c) and 20 min (d) at 623 K. (b) Dark-field TEM image of Ag precipitates (light spots) in the cryo-rolled sample. The numbers 1 and 2 indicate Regions 1 and 2, respectively. (e) is obtained by tilting the specimen in (d) by three degrees. A part of the strained region indicated by the white rectangle in (e) is shown with higher magnification in (f).

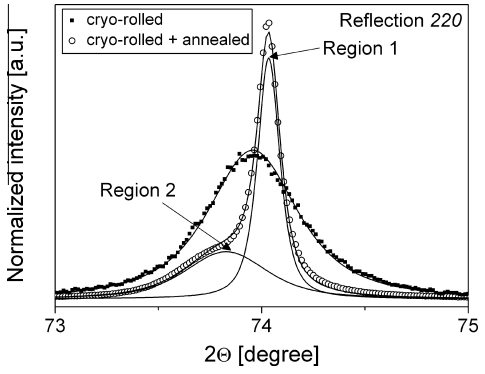

Fig. 3. The eCMWP fitting for reflection (220) of the Cu–3 at.% Ag sample in cryo-rolled state, and after annealing for 20 min at 623 K. The symbols and the solid lines represent the measured data and the fitted curves, respectively. The diffraction peak in the annealed condition is a sum of two reflections related to Regions 1 and 2 having different average lattice parameters (for details see the text). In this figure the integrated intensity (the area under the peak after background subtraction) is normalized to unity for both cryo-rolled and annealed states.

decreased to 0.3 ± 0.1 at.% during the first 10 min of annealing and remained unchanged within the experimental error up to 120 min. This value agrees with the equilibrium Ag concentration in Cu at 623 K (0.33%) within the experimental error. The increase

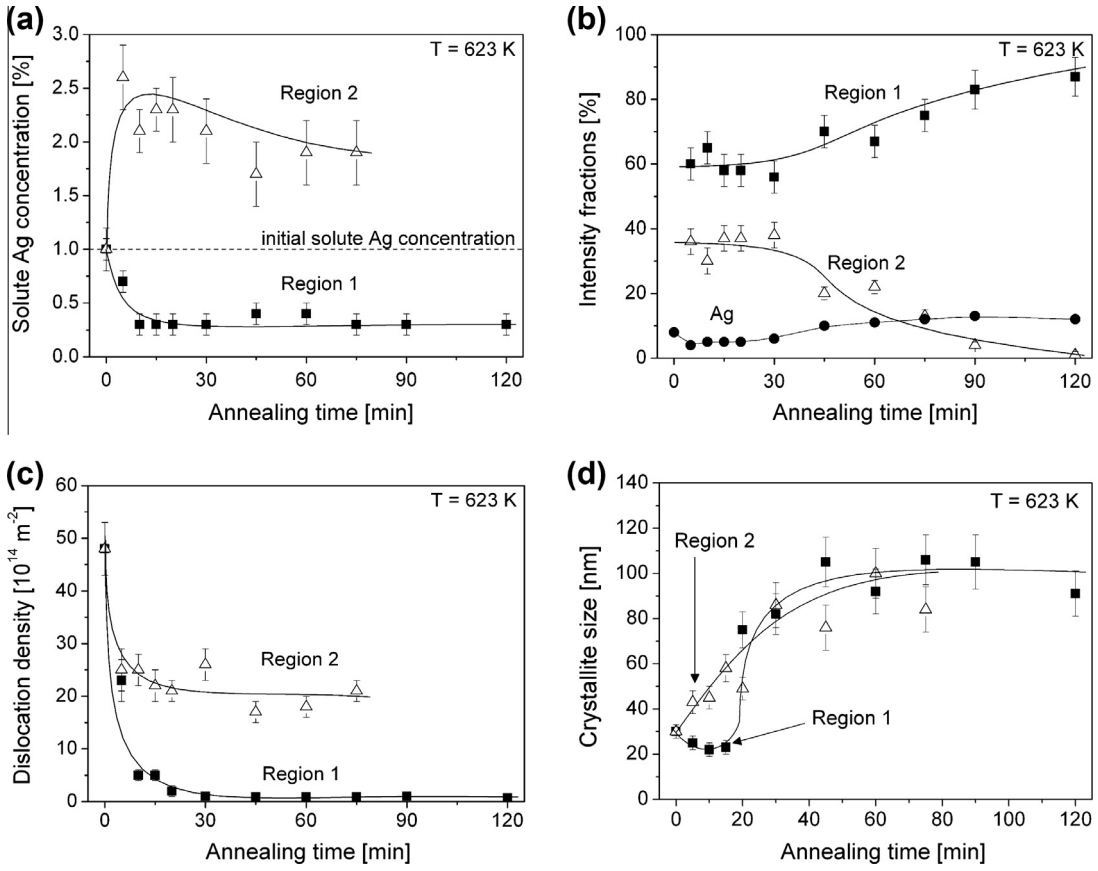

Fig. 4. The variation of the solute Ag concentration (a), the X-ray intensity fraction, (b) the dislocation density (c) and the crystallite size (d) for Regions 1 and 2 in the Cu matrix as a function of annealing time. The solid curves serve only as guide to eyes.

and the decrease of solute Ag concentration during annealing suggest the dissolution and the precipitation of Ag in Regions 2 and 1, respectively.

The changes in the fractions of Regions 1 and 2 in the Cu matrix and the Ag precipitates are described by the variation of the relative diffraction peak intensities of these phases in the X-ray patterns. The sum of the areas under the diffraction peaks (i.e. the integrated intensity) for each phase was determined in the diffraction angle range $2\Theta = 30–140°$. It is noted that the intensity fractions of the different phases do not agree with their volume fractions due to the different atomic scattering factors and densities of Cu and Ag. Fig. 4b shows the X-ray intensity fractions as a function of annealing time. In the cryo-rolled state, the relative intensity of the Ag phase is 8 ± 1% which decreased to 5 ± 1% after 5 min annealing and remained unchanged within the experimental error up to 30 min. This observation is in accordance with the dissolution of Ag precipitates in Region 2. In this period, the fractions of Regions 1 and 2 are ~60% and ~35%, respectively. Between 30 and 120 min the fractions of Regions 1 and 2 increased and decreased, respectively. This indicates that precipitation occurred in Region 2 which reduced the solute Ag concentration to the equilibrium value (~0.3 at.%). After 120 min annealing, the fraction of Region 2 – where the dissolution of Ag had occurred in the beginning of the heat-treatment – was practically zero. Concerning the relative intensity of the Ag phase, it increased gradually to 13 ± 1% between 30 and 120 min in accordance with the reduction of the fraction of the matrix volume with high solute Ag content (Region 2).

The variations in the dislocation density and the crystallite size in Regions 1 and 2 of the Cu matrix as a function of the annealing time were investigated by XLPA. In the fitting of the experimental patterns, each theoretical line profile consisted of two peaks corresponding to the two regions. The dislocation density and the crystallite size in Regions 1 and 2 of the Cu matrix were determined from the fitting and are presented in Fig. 4c and d, respectively. The results reveal that while in Region 1 the dislocation density was reduced by about one order of magnitude in the first 10 min, in Region 2 it decreased only to about half of the initial value due to the stronger pinning effect of the higher solute Ag concentration. Further annealing up to 75 min resulted in only a slight change in the dislocation density in Region 2. This indicates that the dislocation density in Region 2 remained very high ($\sim 20 \times 10^{14}\ m^{-2}$) until this volume transformed to Region 1 by the strong reduction of the solute Ag concentration due to precipitation reaction. Between 75 and 120 min the dislocation density and the crystallite size in Region 2 were not determined since the fraction of this region was very low (<10%) for long annealing times (see Fig. 4b). In Region 1, the dislocation density decreased to $\sim 1 \times 10^{14}\ m^{-2}$ during the first 30 min of annealing, then it remained unchanged within the experimental error up to 120 min. In Region 2, the crystallite size increased during the first 30 min of annealing due to recovery of the microstructure (annihilation and rearrangement of dislocations into low energy configurations), then it remained unchanged with further annealing up to 75 min. It is noted that the dissolution of Ag particles might also contribute to the increase of Cu crystallite size, as the volumes of the former Ag precipitates were occupied by the neighboring Cu crystallites. At the same time, in Region 1 the crystallite size first decreased slightly and it increased only for longer annealing times. The reduction of the Cu crystallite size in the beginning of

heat-treatment is most probably caused by the growth of the neighboring Ag particles (as the solute Ag content decreased). For longer annealing times, the recovery/recrystallization in the matrix might lead to the increment in the Cu crystallite size. The twin boundary probability in both regions of the heat-treated Cu matrix was found to be in the range of 0–0.4% without any clear trend with the variation of annealing time.

The separation of the microstructure into two regions with a low and a high defect density is also confirmed by the TEM images presented in Fig. 2c and d for 10 and 20 min annealing times, respectively. The large grain in the middle of Fig. 2c contains numerous discontinuous Ag precipitates [32] without noticeable lattice strain, while the surrounding regions show strain contrast. Most probably, the former and the latter volumes correspond to Regions 1 and 2, respectively (denoted by the numbers 1 and 2 in Fig. 2c). Similarly, a strained volume without Ag particles can be seen in the upper part of Fig. 2d, while the middle region does not show strain contrast but it contains Ag precipitates. The strain contrast does not change considerably even if the specimen is tilted by three degrees (see Fig. 2e). A part of the strained region indicated by the white rectangle in Fig. 2e is shown with higher magnification in Fig. 2f. Individual dislocations cannot be resolved in these TEM micrographs due to the very high dislocation density. Additional HRTEM analysis revealed a local dislocation density of 10^{16} m^{-2} in the rolled sample annealed for 20 min, however the average dislocation density cannot be determined by this method with good statistics. At the same time, X-ray line profile analysis can provide this very large dislocation density with high reliability. Therefore, the two methods (TEM and X-ray line profile analysis) can be regarded as complementary methods for the microstructure investigation. After annealing for longer times the microstructure becomes more homogeneous in which all Cu grains are coarse and contain discontinuous Ag particles, as illustrated for the sample annealed for 120 min in the TEM image of Fig. 5a. The size of the Cu matrix grains is 1–4 μm (see Fig. 5a) and they contain many elongated Ag precipitates (see the bright- field TEM image in Fig. 5b). The dark-field TEM images shown in Fig. 5c and d were taken from the same area as Fig. 5b but using only Cu and Ag reflections, respectively. Fig. 5d reveals that the elongated Ag precipitates consist of equiaxial grains. The size of 93 Ag grains was determined and the obtained size distribution was fitted by a log-normal function. The median and the log-normal variance of the fitted distribution were $m = 22 \pm 1$ nm and $\sigma^2 = 0.29 \pm 0.01$, respectively.

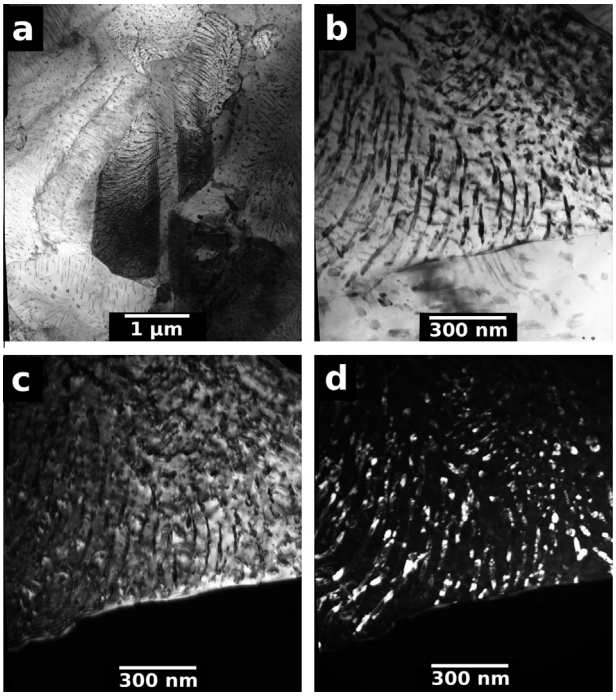

Fig. 5. TEM images of the microstructure after annealing for 120 min at 623 K. (a, b) bright-field images, (c) and (d) dark-field images using Cu and Ag reflections, respectively.

4. Discussion

The decrease of the solute Ag content during annealing in Region 1 can be easily understood since the cryo-rolled alloy with the Ag concentration of ~1% is supersaturated at 623 K (the equilibrium solubility limit is 0.33% at this temperature). It is noted that the solute Ag concentration in Region 1 is 0.3 ± 0.1% for annealing times equal or larger than 10 min (see Fig. 4a) which agrees with the equilibrium value of 0.33% within the experimental error. However, the partial dissolution of Ag precipitates in Region 2 is surprising at first sight. This observation is confirmed by the decrease of the relative X-ray intensity for Ag phase from about 8% to 5% following annealing (see Fig. 4b). The dissolution of Ag precipitates formed during cryo-rolling could be caused by their very small size which yielded an enhanced solubility limit of Ag in Cu. The solubility limit depends on the size of Ag dispersoids as expressed by the Gibbs–Thomson formula (also referred to as Ostwald–Freundlich equation) [33,34]:

$$c_d = c_\infty \exp\left(\frac{6\gamma V_m}{dRT}\right), \quad (1)$$

where d is the diameter of the initial Ag precipitates, T is the temperature of annealing (623 K), c_∞ (0.33 at.%) and c_d are the solute Ag concentrations in the Cu matrix with Ag precipitates having infinitely small curvature (large diameter) and diameter of d, respectively, γ is the interface energy between the Cu matrix and the Ag precipitates, R is the molar gas constant, V_m is the molar volume of Ag (10^{-5} m^3/mole). The value of γ depends on the interface structure. For instance, the energies of semi-coherent (1 1 1)/(1 1 1) and (100)/(100) Ag/Cu interfaces are 0.23 and 0.53 J/m^2, respectively [35]. These values are much lower than that for coherent interfaces (~1 J/m^2) [36]. Previous electron microscopy studies have revealed both cube-on-cube and hetero-twin orientation relationships between Cu and Ag phases separated by semi-coherent interfaces [37–39]. It has also been shown that the size of Ag precipitates influences the nature of interfaces: below 2 nm misfit dislocations – which are characteristic features of semi-coherent boundaries – were not observed in Cu/Ag interfaces, therefore these boundaries were considered to be coherent [14,40]. Electron diffraction experiments carried out on the present sample annealed for 20 min revealed that in Region 1 there is cube-on-cube orientation relationship between Cu and Ag crystallites, as shown in the inset of Fig. 6. The areas with Moiré fringes correspond to the Ag particles grown epitaxially to the Cu crystallites. The Moiré pattern is caused by the difference between the interplanar spacings of (1 1 1) planes in Cu and Ag (the crystallographic direction [12$\bar{3}$] is perpendicular to the image plane). The former and the latter spacings are $d_{Cu} = 0.2087$ and $d_{Ag} = 0.2359$ nm, respectively. According to Ref. [41] the spacing of the resulted translational Moiré fringes (d_M) can be obtained as:

$$d_M = \frac{d_{Ag} d_{Cu}}{d_{Ag} - d_{Cu}}. \quad (2)$$

Eq. (2) yields $d_M = 1.81$ nm which agrees with the experimentally determined value of 1.8 nm, confirming that the areas with Moiré fringes correspond to epitaxially grown Ag particles in the Cu matrix.

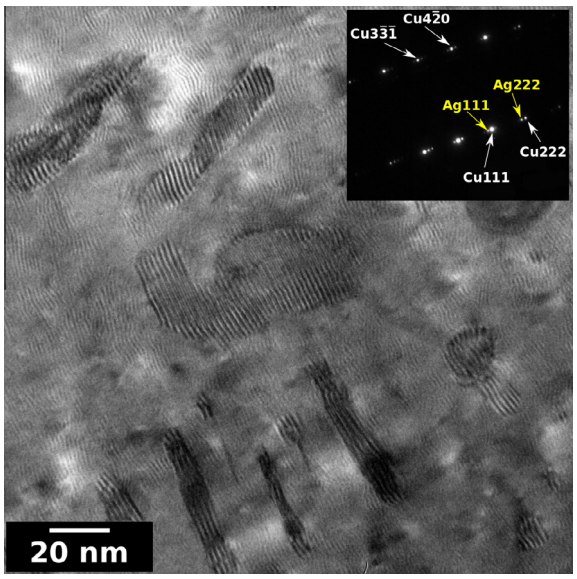

Fig. 6. HRTEM image obtained on the cryo-rolled sample after annealing for 20 min. The selected area diffraction pattern is also shown in the inset. The areas with Moiré fringes correspond to epitaxially grown Cu and Ag crystallites.

Assuming semi-coherent interfaces between Ag and Cu, the arithmetic average of the energies of (111)/(111) and (100)/(100) Ag/Cu interfaces (0.38 J/m^2) was substituted into Eq. (1). According to this formula, the solute Ag concentration in the Cu matrix as a function of the diameter of Ag particles at the temperature of annealing (623 K) is plotted in Fig. 7a (solid line). For precipitate sizes smaller than ~4 nm the value of c_d obtained from Eq. (1) is higher than the average solute Ag concentration measured in the rolled sample (1 at.%). Therefore, the smaller Ag nanoparticles in the size distribution start to dissolve into the Cu matrix during annealing. The size of these small Ag precipitates decreases while the solute Ag concentration in the surrounding Cu matrix increases. The question is whether a particle smaller than ~4 nm will be dissolved totally or after a partial dissolution the process stops since the increased Ag content in the neighboring matrix reaches the solubility corresponding to the size of the partially dissolved Ag particle. A simple model calculation is proposed below for the investigation of this effect.

For the simplicity of the calculation, it was assumed that the Ag particles are spheres in the as-rolled state (see Fig. 2b). Then, the Cu matrix was divided into cubic volumes in such a manner that each cube contains only one Ag particle in its center (see Fig. 8). The length of the edges of the cubes is denoted by D. During dissolution of Ag particles the diameter of the dispersoids decreases from d_0 to d while the solute concentration increases in the matrix cube. The Ag solute concentration in percentage (c_{Ag}) for a given value of d can be calculated as:

$$c_{Ag}(d) = 100 \cdot \frac{\left(D^3 - \frac{d_0^3\pi}{6}\right) \cdot \frac{0.01}{a_{Cu}^3} + \frac{(d_0^3 - d^3)\pi}{6 \cdot a_{Ag}^3}}{\left(D^3 - \frac{d^3\pi}{6}\right) \cdot \frac{1}{a_{Cu}^3}}, \quad (3)$$

where a_{Cu} = 0.3615 nm and a_{Ag} = 0.4086 nm are the lattice parameters of Cu and Ag phases, respectively. The first and the second terms in the numerator of Eq. (3) correspond to the solute Ag concentration in the matrix before annealing (~1 at.%) and the dissolved Ag concentration due to the decrease of the size of Ag precipitates, respectively. The value of D can be obtained from d_0 and the Ag concentration stored in the Ag precipitates in the initial rolled state (~2 at.%) as:

$$D^3 = \frac{d_0^3\pi}{6 \cdot 0.02} \cdot \frac{a_{Cu}^3}{a_{Ag}^3}. \quad (4)$$

The dashed lines in Fig. 7a show the evolution of the Ag concentration with decreasing the size of Ag particles for the initial precipitate diameters of d_0 = 2 and 3 nm in the case of γ = 0.38 J/m^2. The intersection of the dashed and solid curves denoted by solid circle corresponds to the case when the Ag concentration around the partially dissolved precipitate agrees with the equilibrium value c_d corresponding to the actual Ag particle size d. Then, the dissolution stops as illustrated for the precipitate diameter of 3 nm in Fig. 7a. However, the Ag precipitates smaller than ~3 nm (e.g. 2 nm in Fig. 7a) are dissolved totally which yields a relatively large increase of the solute Ag concentration in Region 2 of the Cu matrix. It is noted that the particles with the size between 3 and 4 nm can also be dissolved totally if the solute Ag atoms diffuse quickly away from these particles to the volumes with low Ag concentration (e.g. to Region 1).

Fig. 7b shows the solute Ag concentration in the Cu matrix as a function of the diameter of Ag particles at 623 K for coherent interfaces. Due to the higher interface energy (~1 J/m^2) compared to the semi-coherent case, the particle size limit of dissolution is larger here (10 nm). The dashed lines obtained according to Eq. (3) indicate that the Ag precipitates smaller than 8 nm (e.g. 6 nm in Fig. 7b) are totally dissolved during annealing at 623 K. Therefore, the volumes where the dissolution of Ag precipitates occurred during annealing (Region 2) are most probably the regions in which the Ag particles have very small size and/or large specific interface energy.

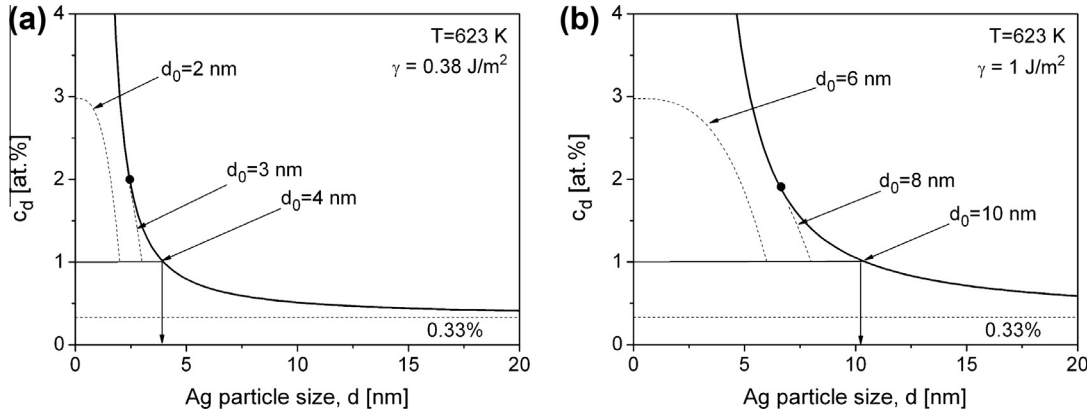

Fig. 7. The equilibrium Ag solute concentration in the Cu matrix as a function of the size of Ag nanoparticles at 623 K for two interface energies of (a) 0.38 and (b) 1 J/m^2. The dashed lines indicate the evolution of the solute concentration if Ag particles with the initial size of d_0 were dissolved in the Cu matrix.

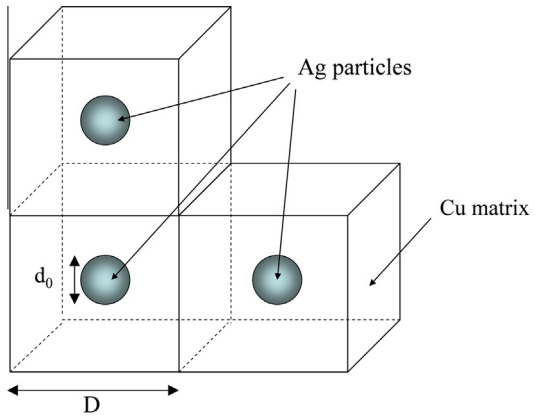

Fig. 8. The model used for the calculation of Ag concentration in the Cu matrix in the vicinity of partially dissolved Ag particles with the initial size of d_0.

In Region 1, the decrease of solute Ag concentration could occur by the growth of the existing Ag particles. In this case, the size of Cu crystallites between the Ag particles should decrease which is in accordance with the results of XLPA for short annealing periods (see Fig. 4d). For longer annealing times ($\geqslant$20 min), the Cu crystallite size in Region 1 started to increase most probably due to a strong recovery and/or recrystallization. In Region 2, both the dissolution of Ag precipitates and the recovery/recrystallization in the Cu matrix yielded an increment in Cu crystallite size.

Due to the spatially heterogeneous dissolution, an inhomogeneous dislocation structure was also developed in the Cu matrix during annealing. In Region 1, the dislocation density strongly decreased due to the reduced solute Ag atom content while in region 2 the dislocation density remained relatively high in the Cu matrix owing to the pinning effect of the increased solute Ag concentration. This heterogeneous microstructure yielded an improvement of the ductility while retaining the high strength of the annealed material as shown in our previous paper [17].

This study also reveals the thermal stability of the partially recovered/recrystallized microstructure during annealing the cryo-rolled Cu–3 at.% Ag alloy. Fig. 4 shows that the high dislocation density and the large volume fraction of Region 2 remained up to 30 min during annealing at 623 K. This means that the combination of high strength and good ductility caused by the bimodal microstructure (see [17]) is expected to be retained till the end of this period. Additional investigations are needed to reveal the mechanical behavior as a function of annealing time. It is noted that a relatively large dislocation density (1×10^{14} m^{-2}) remained in the Cu matrix even after annealing for 120 min. Misfit dislocations between Cu and Ag phases probably contribute to this dislocation density and these dislocations are structurally necessary in the semi-coherent Cu/Ag interfaces [40,42]. It is also worth to note that the route and the strain of SPD-processing most probably influence the size and interface energy of Ag precipitates, i.e. SPD can be applied for interface engineering. Therefore, the functional properties (strength, ductility, conductivity, etc.) of Cu–Ag alloys can be tuned by an appropriate selection of the SPD-processing conditions, the chemical composition, as well as the time and temperature of annealing.

5. Conclusions

Supersaturated Cu–3 at.% Ag alloy was subjected to cold rolling and subsequent annealing at 623 K up to 120 min. The effect of this heat-treatment on the microstructure was investigated and the following conclusions have been drawn:

1. Shortly after the beginning of annealing (in 5 min) an inhomogeneous solute atom distribution developed in the Cu matrix due to the dissolution of Ag nanoparticles in the regions where the Ag particles have very small size (a few nanometer) and/or large specific interface energy with the Cu matrix. In other volumes, the solute Ag concentration decreased to the equilibrium value by discontinuous precipitation reaction.
2. In the region where the Ag solute content was reduced, the dislocation density developed during cryo-rolling decreased by more than one order of magnitude, while in the regions where the solute concentration increased the dislocation density in the Cu matrix was reduced only to half of the value obtained after cryo-rolling. Therefore, the samples annealed after cryo-rolling exhibited heterogeneous microstructures where both the dislocation density and the solute concentration varied considerably.
3. The region in which dissolution occurred exhibited good thermal stability since its fraction (about 35%) with large dislocation density and high solute Ag content remained unchanged up to 30 min at 623 K. With continued annealing, the volume fraction of this region gradually decreased and after 120 min annealing it became practically zero, resulting in a homogeneous equilibrium Cu matrix with discontinuous Ag precipitates.

Acknowledgements

This work was supported by the Hungarian Scientific Research Fund, OTKA, Grant No. K-109021. The authors are grateful to Ms. Noémi Szász for the preparation of the TEM lamellae. A.K. and J.F. gratefully acknowledge funding by the Deutsche Forschungsgemeinschaft FR 1714/5-1.

References

[1] R.Z. Valiev, T.G. Langdon, Principles of equal-channel angular pressing: a processing tool for grain refinement, Prog. Mater. Sci. 51 (2006) 881–981.
[2] A.P. Zhilyaev, T.G. Langdon, Using high-pressure torsion for metal processing: fundamentals and applications, Prog. Mater. Sci. 53 (2008) 893–979.
[3] J. Gubicza, N.Q. Chinh, Gy. Krállics, I. Schiller, T. Ungár, Microstructure of ultrafine-grained fcc metals produced by severe plastic deformation, Curr. Appl. Phys. 6 (2006) 194–199.
[4] R. Kuzel, M. Janecek, Z. Matej, J. Cizek, M. Dopita, O. Srba, Microstructure of equal-channel angular pressed Cu and Cu–Zr samples studied by different methods, Metall. Mater. Trans. A 41 (2010) 1174–1190.
[5] H.S. Kim, W.Y. Kim, K.H. Song, Effect of post-heat-treatment in ECAP processed Cu–40%Zn brass, J. Alloys Comp. 536 (2012) S200–S203.
[6] T.H. Courtney, Mechanical Behavior of Materials, second ed., Waveland Press, Long Grove, 2005.
[7] W. Soboyejo, Mechanical Properties of Engineered Materials, Marcel Dekker, New York, 2003.
[8] J. Gubicza, N.Q. Chinh, Z. Horita, T.G. Langdon, Effect of Mg addition on microstructure and mechanical properties of aluminum, Mater. Sci. Eng. A 387–389 (2004) 55–59.
[9] C.M. Cepeda-Jiménez, J.M. Garcia-Infanta, A.P. Zhilyaev, O.A. Ruano, F. Carreno, Influence of the supersaturated silicon solid solution concentration on the effectiveness of severe plastic deformation processing in Al–7 wt.% Si casting alloy, Mater. Sci. Eng. A 528 (2011) 7938–7947.
[10] N. Tsuji, Y. Ito, Y. Saito, Y. Minamino, Strength and ductility of ultrafine-grained aluminum and iron produced by ARB and annealing, Scr. Mater. 47 (2002) 893–899.
[11] Y. Wang, M. Chen, F. Zhou, E. Ma, High tensile ductility in a nanostructured metal, Nature 419 (2002) 912–915.
[12] T. Shanmugasundaram, V. Subramanya Sarma, B.S. Murty, M. Heilmaier, High strength bulk nanostructured 2219 Al alloy produced by high energy ball milling and hot pressing, Mater. Sci. Forum 584–586 (2008) 97–101.
[13] Y. Sakai, H.-J. Schneider-Muntau, Ultra-high strength, high conductivity Cu–Ag alloy wires, Acta Mater. 45 (1997) 1017–1023.
[14] S.I. Hong, M.A. Hill, Microstructural stability and mechanical response of Cu–Ag microcomposite Wires, Acta Mater. 46 (1998) 4111–4122.
[15] J. Freudenberger, High strength copper-based conductor materials, in: M. Naboka, J. Giordano (Eds.), Copper Alloys: Preparation, Properties and Applications, Nova Science Publishers, New York, 2011, pp. 159–212.
[16] Y.Z. Tian, S.D. Wu, Z.F. Zhang, R.B. Figueiredo, N. Gao, T.G. Langdon, Comparison of microstructures and mechanical properties of a Cu–Ag alloy

processed using different severe plastic deformation modes, Mater. Sci. Eng. A 528 (2011) 4331–4336.
[17] K. Sitarama Raju, V. Subramanya Sarma, A. Kauffmann, Z. Hegedűs, J. Gubicza, M. Peterlechner, J. Freudenberger, G. Wilde, High strength and ductile ultrafine grained Cu–Ag alloy through bimodal grain size, dislocation density and solute distribution, Acta Mater. 61 (2013) 228–238.
[18] Y.Z. Tian, J. Freudenberger, R. Pippan, Z.F. Zhang, Formation of nanostructure and abnormal annealing behavior of a Cu–Ag–Zr alloy processed by high-pressure torsion, Mater. Sci. Eng. A 568 (2013) 184–194.
[19] Y.G. Ko, S. Namgung, B.U. Lee, D.H. Shin, Mechanical and electrical responses of nanostructured Cu–3 wt%Ag alloy fabricated by ECAP and cold rolling, J. Alloys Comp. 504S (2010) S448–S451.
[20] J. Nelson, J.D. Riley, An experimental investigation of extrapolation methods in the derivation of accurate unit cell dimension of crystals, Proc. Phys. Soc. Lond. 57 (1945) 160–177.
[21] G. Ribárik, J. Gubicza, T. Ungár, Correlation between strength and microstructure of ball milled Al–Mg alloys determined by X-ray diffraction, Mater. Sci. Eng. A 387–389 (2004) 343–347.
[22] J. Gubicza, X-ray Line Profile Analysis in Materials Science, IGI-Global, Hershey, 2014.
[23] M. Wilkens, Theoretical aspects of kinematical X-ray diffraction profiles from crystals containing dislocation distributions, in: J.A. Simmons, R. de Wit, R. Bullough (Eds.), Fundamental Aspects of Dislocation Theory, National Bureau of Standards, Washington, DC, 1970, pp. 1195–1221.
[24] L. Balogh, G. Ribárik, T. Ungár, Stacking faults and twin boundaries in fcc crystals determined by X-ray diffraction profile analysis, J. Appl. Phys. 100 (2006) 023512.
[25] J.L. Lábár, Consistent indexing of a (set of) SAED pattern(s) with the process diffraction program, Ultramicroscopy 103 (2005) 237–249.
[26] J. Song, H. Li, J. Li, S. Wang, S. Zhou, Fabrication and optical properties of metastable Cu–Ag alloys, Appl. Opt. 41 (2002) 5413–5416.
[27] J. Gubicza, I. Schiller, N.Q. Chinh, J. Illy, Z. Horita, T.G. Langdon, The effect of severe plastic deformation on precipitation in supersaturated Al–Zn–Mg alloys, Mater. Sci. Eng. A 460–461 (2007) 77–85.
[28] Y.H. Zhao, X.Z. Liao, Z. Horita, T.G. Langdon, Y.T. Zhu, Determining the optimal stacking fault energy for achieving high ductility in ultrafine-grained Cu–Zn alloys, Mater. Sci. Eng. A 493 (2008) 123–129.
[29] D. Setman, E. Schafler, E. Korznikova, M.J. Zehetbauer, The presence and nature of vacancy type defects in nanometals detained by severe plastic deformation, Mater. Sci. Eng. A 493 (2008) 116–122.
[30] J. Gubicza, S.V. Dobatkin, E. Khosravi, A.A. Kuznetsov, J.L. Lábár, Microstructural stability of Cu processed by different routes of severe plastic deformation, Mater. Sci. Eng. A 528 (2011) 1828–1832.
[31] J. Gubicza, Defect Structure in Nanomaterials, Woodhead, Cambridge, 2012.
[32] J. Lin, L. Meng, Effect of aging treatment on microstructure and mechanical properties of Cu–Ag alloys, J. Alloys Comp. 454 (2008) 150–155.
[33] M. Perez, Gibbs–Thomson effect in phase transformations, Scr. Mater. 52 (2005) 709–712.
[34] G. Kaptay, Nano-Calphad: extension of the Calphad method to systems with nano-phases and complexions, J. Mater. Sci. 47 (2012) 8320–8335.
[35] P. Bacher, P. Wynblatt, S.M. Foiles, A Monte Carlo study of the structure and composition of (001) semicoherent interphase boundaries in Cu–Ag–Au alloys, Acta Metall. Mater. 39 (1991) 2681–2691.
[36] F.J. Delogu, Free energy differences between Ag−Cu nanophases with different chemical order, J. Phys. Chem. C 114 (2010) 19946–19951.
[37] K. Han, A.A. Vasquez, Y. Xin, P.N. Kalu, Microstructure and tensile properties of nanostructured Cu–25 wt%Ag, Acta Mater. 51 (2003) 767–780.
[38] J.B. Liu, Y.W. Zeng, L. Meng, Interface structure and energy in Cu–71.8 wt.% Ag, J. Alloys Comp. 464 (2008) 168–173.
[39] Y.Z. Tian, Z.F. Zhang, Bulk eutectic Cu–Ag alloys with abundant twin boundaries, Scr. Mater. 66 (2012) 65–68.
[40] J.B. Liu, L. Zhang, D.W. Yao, L. Meng, Microstructure evolution of Cu/Ag interface in the Cu–6 wt.% Ag filamentary nanocomposite, Acta Mater. 59 (2011) 1191–1197.
[41] D.B. Williams, C.B. Carter, Transmission Electron Microscopy, Springer, New York, 2009.
[42] J.B. Liu, L. Meng, Phase orientation, interface structure, and properties of aged Cu–6wt.% Ag, J. Mater. Sci. 43 (2008) 2006–2011.